Atomistic SPH and a Link between Diffusion and Interfacial Tension

Ludwig C. Nitsche and Weidong Zhang
Dept. of Chemical Engineering, University of Illinois at Chicago, Chicago, IL 60607

The mesh-free method of smoothed particle hydrodynamics (SPH) is interpreted atomistically to treat the local density of nodes as representing solute concentration, instead of interpolating a concentration field between function values at the nodes. We exploit the conceptual simplicity of tracking little packets (representing supermolecular aggregates) of solute, as in Brownian dynamics simulations, but replace the stochastic generation of diffusive spreading over statistically independent realizations with a purely deterministic summation for extracting the local diffusion velocity using only the instantaneous locations of nearby nodes. Four test problems demonstrate the versatility and accuracy of the atomistic SPH method (ASPH) for mass transfer. Finally, by comparing ASPH with a new Stokeslet-swarm technique for simulating drop flows (Nitsche and Schaflinger, 2001), a fundamental analogy between diffusion and interfacial tension is exposed.

Introduction

From engineering to astrophysics, the complexity of grid generation has driven a trend toward mesh-free methods for solving PDEs. New ways have been found to interpolate between nodal solution values without actually having to connect the nodes together into a mesh. In one form or another (Dilts, 1999; Oñate et al., 1996a,b; Belytschko et al., 1998), such methods are usually related to the elegant approach of smoothed particle hydrodynamics or SPH (Gingold and Monaghan, 1977; Monaghan, 1992), whereby a discrete, summed version of a convolution integral—involving a localized weight function or kernel—provides interpolated function values and spatial derivatives. The classical numerical methods (finite-difference, finite-element, finite-volume) can all be recast in meshless terms (Oñate et al., 1996a), which has advantages in following material deformations (Dilts, 1999; Bonet and Kulasegaram, 2000).

Two recent articles (Cleary and Monaghan, 1999; Chen et al., 1999) report on the application of SPH to heat-transfer problems. In the context of scalar transport, which is of particular interest to chemical engineers, the purpose of this article is to use SPH as the starting point for introducing one final (and very basic) conceptual simplification: to walk away entirely from the idea of interpolating between solute concentrations regarded as function values at the nodes, and let the local density of nodes represent solute concentration. The nodes become oversized, stylized "atoms" or "molecules" that get moved around by the appropriate (macroscopic) fluxes.

Of course, in traditional SPH the nodes can move as well, but then they still only represent *roving places used to record values of the concentration field, as opposed to representing the bits of matter that make up the quantity of concentration itself*. In summary, traditional SPH keeps track of both the coordinates of the nodes and the concentration values at those locations. The atomistic version advanced here (ASPH) uses only the nodal coordinates in what is effectively a stylized, oversized molecular simulation.

Tracking little packets of a conserved quantity (mass, momentum, energy) that essentially "take care of themselves" without the intervention of a numerical analyst is not a new idea: it is the basis of stochastic simulations (Wedgewood and Guerts, 1995; Grassia et al., 1995). Particularly in the literature of polymer rheology, Brownian dynamics (BD) has long been the only practical method of dealing with the many degrees of freedom of polymer chains (Öttinger, 1996). The bottleneck, of course, lies in the statistics. Long times, or large ensembles, are required to let the random fluctuations that model diffusion (in a stylized way) settle down.

Correspondence concerning this article should be addressed to L. C. Nitsche.

Given an instantaneous ensemble of particles, we do not, however, have to wait to see how the (independent) random walks of all simultaneously will redistribute them *a la* BD. The lesson from SPH, as interpreted here, is that we should be able to determine the local diffusion velocity of each particle in the ensemble directly from the instantaneous locations of its near neighbors. (By diffusion velocity, we mean the *macroscopic* velocity $\boldsymbol{v}_{\{c\}} = \boldsymbol{J}/c$ associated with the flux $\boldsymbol{J}$ of solute, which filters out the microscale statistical fluctuations that cause diffusion.) For this, we must be able to calculate both the concentration and its gradient at any point, which the SPH weight function allows us to do. The weight function is equivalent in basic action to a stylized intermolecular potential.

Prototypical of the particulate approach to extracting space-derivative information is the technique of Nitsche and Schaflinger (2001) for estimating the mean curvature at the fuzzy interface of a macroscopic drop made from a suspension of particles. A suitable potential (weight function) obviated the need to deal explicitly with the interface at all in the course of the simulations. In contrast with both ASPH and molecular dynamics (MD), the pseudo-molecular forces acting upon the particles were "run through" a convolution product with the Green's function for Stokes flow. In other words, the particles did not interact directly through the forces, but *indirectly* through the continuum flow fields (Stokeslets) set in motion by those forces (Machu, 2001; Machu et al., 2001). This formulation has a direct link to the (continuum-level) boundary-integral equations for Stokes flow of drops (Rallison and Acrivos, 1978; Pozrikidis, 1992).

ASPH does not employ the intervening "layer" of a Green's function, because it treats scalar transport by advection and diffusion, and not the underlying hydrodynamics. Thus, ASPH works essentially like a molecular simulation that has been coarse-grained (by lumping molecules into aggregates) to model macroscopic scales of length and time. However, the underlying premise differs fundamentally from MD: the trajectories represent only *continuum-level* presence and flux of solute, so they are not only deterministic but also—in principle and in some numerical cases—reversible. In contrast, round-off errors are actually beneficial in MD for the molecular trajectories to "forget" their initial conditions, so that irreversible thermodynamic equilibration can occur. In short, MD is always accompanied by microscopic irreversibility due to unavoidable round-off errors, whereas ASPH mimicks irreversible diffusion with continuum-scale trajectories that can—in numerical practice—be reversible on a *macroscopic* timescale. We note that a direct scaling up of MD by lumping molecules together into "quasimolecules" has already been used for simulating macroscopic drops (Greenspan, 1990). Here, we extend this basic idea to scalar transport (advection-diffusion) and show that there is considerable latitude with regard to the weight function: it is constrained more by macroscopic algorithmic considerations than by any resemblance to realistic intermolecular potentials.

Dissipative particle dynamics (DPD) explicitly model mesoscopic fluctuations by adding to the conservative interparticle forces from MD both dissipative and random contributions—a relation between these being imposed by the fluctuation-dissipation theorem. The originators (Hoogerbrugge and Koelman, 1992; Koelman and Hoogerbrugge, 1993) modeled flow around obstacles and shear flow of suspensions. Since then, DPD has fairly exploded onto the particle-simulation scene: hydrodynamic applications include phase separation (Coveney and Novik, 1996) and drop dynamics (Jones et al., 1999; Clark et al., 2000). Extensions to thermal transport have been achieved by regarding each particle as its own thermodynamic entity, and supplementing its position and momentum with temperature as an additional internal variable (Español, 1997b; Avalos and Mackie, 1997; Flekkoy and Coveney, 1999; Mackie et al., 1999). Illustrative references treating conceptual underpinnings, generalizations, and relations to SPH are Español (1995, 1997a, 1998) and Flekkoy and Coveney (1999).

In general terms, the source of diffusive spreading in the aforementioned four classes of particle methods can be distinguished as follows:

- *BD*. Noninteracting particles (statistical ensemble), artificial random fluctuations.
- *ASPH*. Deterministic interparticle forces, no random fluctuations.
- *DPD*. Deterministic interparticle forces plus artificial random fluctuations.
- *MD*. Deterministic intermolecular forces plus random fluctuations (operative over *many* time steps) from numerical round-off errors.

The additional interparticle summations in ASPH must be weighed against the realizations required for accurate statistical convergence in BD. We are looking ahead to a specific application in which ASPH should have a distinct advantage over BD: adding diffusion to the aforementioned Stokeslet-swarm simulations of drop flows at low Reynolds numbers (Machu, 2001; Machu et al., 2001) to treat diffusion in miscible drops. Since all particles are required to interact with each other just to produce the Stokes flow field, we would prefer a method that can extract the diffusion velocities from the instantaneous configuration of the swarm. This topic will be addressed under "A Unified Framework for Diffusion and Interfacial Tension."

The complexity of DPD is necessary to model fluctuations on the mesoscopic scale. However, if all we seek to capture is the resultant, cumulative effect of those fluctuations (as accessible to the continuum-level concentration field governed by the advection-diffusion equation), then the simplicity of ASPH suffices and is computationally preferable.

Background: Averaging with a Weight-Function

Given the concentration field $c(\boldsymbol{r},t)$ of a particular solute within an n-dimensional domain $\mathfrak{D}$, we begin with a local weight-function average as used in SPH (Monaghan, 1992; Chen et al., 1999)

$$\bar{c}(\boldsymbol{r},t;\epsilon) = \left[F(\boldsymbol{r};\epsilon)\right]^{-1} \int_{\mathfrak{A}(\boldsymbol{r};\epsilon)\cap\mathfrak{D}} c(\boldsymbol{q},t) W\left[\epsilon^{-1}(\boldsymbol{q}-\boldsymbol{r})\right] d^n q, \tag{1}$$

with

$$F(\boldsymbol{r};\epsilon) = \int_{\mathfrak{A}(\boldsymbol{r};\epsilon)\cap\mathfrak{D}} W\left[\epsilon^{-1}(\boldsymbol{q}-\boldsymbol{r})\right] d^n q. \tag{2}$$

Here $W(\boldsymbol{r})$ is a continuous weight function that vanishes outside the dimensionless averaging zone $\mathfrak{A}(\mathbf{0};1)$ centered at the origin $\mathbf{0}$. In two dimensions convenient choices for $\mathfrak{A}(\mathbf{0};1)$ would be the unit disc or a square extending between $x, y = \pm 1$. We shift the center of $\mathfrak{A}(\mathbf{0};1)$ to $\boldsymbol{r}$ and shrink (in a geometrically similar fashion) its characteristic dimension down to the filtering lengthscale ϵ to obtain $\mathfrak{A}(\boldsymbol{r};\epsilon)$. In evaluating the gradient of the smoothed concentration field, the operation of differentiation is transferred to the weight function. However, when the averaging zone extends partly outside the domain, something more must be done to correct the spurious impression of a steep gradient presented by the abrupt fall-off in nodal density beyond the boundary. Chen et al. (1999) have derived a suitable correction factor (modified denominator) for the boundary regime, starting from a local Taylor expansion of the function being interpolated. By the same line of reasoning we obtain instead an additive boundary correction

$$\nabla\bar{c}(\boldsymbol{r};\epsilon) = \left[F(\boldsymbol{r};\epsilon)\right]^{-1}\left\{-\epsilon^{-1}\int_{\mathfrak{A}(\boldsymbol{r};\epsilon)\cap\mathfrak{D}} \nabla W\left[\epsilon^{-1}(\boldsymbol{q}-\boldsymbol{r})\right]c(\boldsymbol{q},t)\,d^n q + \bar{c}(\boldsymbol{r};\epsilon)\boldsymbol{G}(\boldsymbol{r};\epsilon)\right\}, \quad (3)$$

with

$$\boldsymbol{G}(\boldsymbol{r};\epsilon) = \int_{\mathfrak{A}(\boldsymbol{r};\epsilon)\cap\partial\mathfrak{D}} W\left[\epsilon^{-1}(\boldsymbol{q}-\boldsymbol{r})\right]\boldsymbol{n}[\boldsymbol{q}]\,d^{n-1}q \quad (4)$$

[see also Campbell (1989)]. Here $\boldsymbol{n}$ is the outward-directed unit normal vector on the boundary $\partial\mathfrak{D}$. In the boundary regime $\bar{c}(\boldsymbol{r},t;\epsilon)$ and $\nabla\bar{c}(\boldsymbol{r},t;\epsilon)$ differ at order ϵ from $c(\boldsymbol{r},t)$ and $\nabla c(\boldsymbol{r},t)$, respectively. Away from the boundaries, the error appears only at order ϵ^2, provided that the weight function is suitably symmetric (Chen et al., 1999).

Atomistic Representation: Something New

As phrased for mass transfer, SPH methods would use Eq. 1 as a means of *interpolating between concentration values* c_m recorded at the discrete nodes $\boldsymbol{r}_m$, to which are attributed the respective elements of measure (volume, area, length) δ_m

$$\hat{c}_{\mathrm{SPH}}(\boldsymbol{r},t;\epsilon) \approx \sum_m c_m(t) W\left[\epsilon^{-1}(\boldsymbol{r}_m - \boldsymbol{r}\,)\right]\delta_m. \quad (5)$$

A caret ($\hat{}$) is used to indicate that an additional level of approximation is involved in replacing the integral 1 with a summation. The nodes may move around to follow the flux of solute [$\boldsymbol{r}_m = \boldsymbol{r}_m(t)$, $\delta_m = \delta_m(t)$], but they function primarily as *positions used to record the concentration.* Note that the δ_m require some kind of meshing to calculate, even though SPH itself does not use the mesh (Duarte, 1995; Cleary and Monaghan, 1999).

Motivated by recent Stokeslet-swarm simulations of drops (Machu, 2001; Machu et al., 2001; Nitsche and Schaflinger, 2001), we shall go one step further in concept and *use only the information in the nodal positions to extract the local concentration.* In this stylized atomistic view, each node plays the role of a tiny agglomerate of many solute molecules lumped together. *Then, we can discard entirely the idea of interpolating the concentration field between the nodal values $c_m(t)$, and simply let the local abundance or scarcity of nodes represent the concentration*

$$\hat{c}_{\mathrm{ASPH}}(\boldsymbol{r},t;\epsilon) \approx \left[F(\boldsymbol{r},t;\epsilon)\right]^{-1}\sum_m W\left[\epsilon^{-1}(\boldsymbol{r}_m(t)-\boldsymbol{r})\right]. \quad (6)$$

This is the essence of the atomistic SPH method (ASPH) proposed here. In the literature of SPH we have found only one mention of this usage of the weight function: the density regarded as an expectation value for randomly distributed nodes in compressible-flow models from astrophysics (Gingold and Monaghan, 1982). Surprisingly, this idea was then *not followed up on* when it came to scalar transport (Cleary and Monaghan, 1999; Chen et al., 1999). It will now require a fair number of nodes spattered over a local smoothing zone $\mathfrak{A}(\boldsymbol{r}_m;\epsilon)$ to approximate the information contained in just one nodal concentration c_m. This disadvantage, however, is outweighed by the conceptual appeal of the atomistic view, which translates into a simpler computational scheme than those developed thus far.

Diffusion Velocity in a Swarm of Nodes

In the advection-diffusion equation (Bird et al., 2002, Chap. 19),

$$\frac{\partial c}{\partial t} + \nabla\cdot\boldsymbol{J} = 0, \quad (7)$$

the flux $\boldsymbol{J}$ of one solute in a dilute liquid solution can be written in terms of a total species velocity $\boldsymbol{v}_{\{c\}}$ that incorporates both "piggy-back" transport due to the local fluid velocity vector $\boldsymbol{u}$, and diffusion down the concentration gradient

$$\boldsymbol{J} = \boldsymbol{u}c - D\nabla c = \boldsymbol{v}_{\{c\}}c \quad (8)$$

with

$$\boldsymbol{v}_{\{c\}}(\boldsymbol{r},t) = \boldsymbol{u}(\boldsymbol{r},t) - D(\boldsymbol{r},t)\left[c(\boldsymbol{r},t)\right]^{-1}\nabla c(\boldsymbol{r},t). \quad (9)$$

In the continuum limit there is a fundamental equivalence between the mapping of material points of solute,

$$\frac{D\boldsymbol{r}}{Dt} = \boldsymbol{v}_{\{c\}}(\boldsymbol{r},t), \quad (10)$$

and the conservation law 7,

$$\frac{\partial c}{\partial t} + \nabla\cdot\left[\boldsymbol{v}_{\{c\}}c\right] = 0. \quad (11)$$

The *ansatz* of ASPH is to track only a finite sampling of material points, and to apply two levels of approximation to calculate their diffusion velocities: using the integral-averaged concentration $\bar{c}$ from Eq. 1 in place of the local concentration c in Eq. 9; and $\hat{c}$ given by the summation formula 6 in place of $\bar{c}$.

Substituting the discrete analogue of Eq. 3 according to Eq. 6, we then find for the species velocity at each node

$$\boldsymbol{v}_m(\boldsymbol{r}_1,\ldots,\boldsymbol{r}_M)=\boldsymbol{u}(\boldsymbol{r}_m,t)+D(\boldsymbol{r}_m,t)\left\{-\left[F(\boldsymbol{r}_m;\epsilon)\right]^{-1}\boldsymbol{G}(\boldsymbol{r}_m;\epsilon)+\epsilon^{-1}\left(\sum_n W\left[\epsilon^{-1}(\boldsymbol{r}_n-\boldsymbol{r}_m)\right]\right)^{-1}\sum_n \nabla W\left[\epsilon^{-1}(\boldsymbol{r}_n-\boldsymbol{r}_m)\right]\right\} \tag{12}$$

Now we simply have to move each node with the local species velocity, and they will collectively represent the movement of solute

$$\frac{d\boldsymbol{r}_m}{dt}=\boldsymbol{v}_m(\boldsymbol{r}_1,\ldots,\boldsymbol{r}_M),\quad m=1,\ldots,M. \tag{13}$$

Leaving aside the advective term, we see that the linear, stochastic representation of diffusion in Brownian dynamics (Grassia et al., 1995; Wedgewood and Guerts, 1995; Öttinger, 1996) has been replaced with a nonlinear but deterministic dynamical system in ASPH. In the numerator in Eq. 12, ∇W responds to variations in the nodal density about its center: where there is an imbalance, it pushes from higher toward lower density.

Equation 12 represents the local flux vector $\boldsymbol{J}$, not its divergence (which involves second partial derivatives of concentration). This constitutes a significant conceptual shortcut compared with previous applications of SPH to scalar transport (Cleary and Monaghan, 1999; Chen et al., 1999)—particularly because now discontinuous coefficients require no special handling. Furthermore, the question of a conservative formulation is irrelevant: nodes simply get moved around by the local species velocities, but they cannot spontaneously appear or disappear as a numerical defect buried in the discretization error. Things just take care of themselves.

Numerical Implementation

A swarm of Stokeslets gave an immediate visual representation (without post processing) of the shape evolution of a drop (Machu, 2001; Machu et al., 2001; Nitsche and Schaflinger, 2001). Indeed, it represented a coarse version of what was actually seen in the laboratory in the case of suspension drops. Packet-based computer simulations enjoy a similar advantage when visualizing the results for scalar transport problems. The atomistic nodes immediately give a stippled equivalent of a contour plot. Equation 6 yields the local number density of nodes at any point $\boldsymbol{r}$. This must be renormalized to give concentration in dimensionless units, independent of the total number M of nodes.

Time stepping

For solving the coupled, nonlinear ODE system (Eqs. 12 and 13) numerically, a second-order scheme suffices to prevent nodes spiraling out systematically toward the convex side of curved streamlines (Hinch, private communication). For our test problems, good results were obtained using a second-order Runge Kutta scheme with fixed-time step. More sophisticated predictor-corrector schemes have been used with SPH (Monaghan, 1992; Cleary and Monaghan, 1999).

Adaptive refinement

The averaging lengthscale ϵ appears explicitly in the above equations in order to emphasize that the size of the averaging zone $\mathfrak{A}(\boldsymbol{r};\epsilon)$ should be adjusted to reflect the local density of nodes (Monaghan, 1992). A good rule of thumb is to keep the number $N(\boldsymbol{r},\epsilon)$ of nodes covered by $\mathfrak{A}(\boldsymbol{r};\epsilon)$ roughly fixed at a target value N^*, irrespective of the position $\boldsymbol{r}$ [see the adaptive SPH scheme of Serna et al. (1996)]. In the two-dimensional test problems to be described below, $\mathfrak{A}(\boldsymbol{r};\epsilon)$ consisted of either a circle of radius ϵ or a square of side-length 2ϵ centered at $\boldsymbol{r}=(x,y)$. A simple binary chop was used to zero in on the local size $\epsilon(x,y)$ that included the desired number of nodes (approximately, within a prescribed tolerance). We also experimented with an iterative scheme.

Pure Diffusion

First, we consider pure diffusion in the (x,y) plane

$$\frac{\partial c}{\partial t}=\frac{\partial^2 c}{\partial x^2}+\frac{\partial^2 c}{\partial y^2}, \tag{14}$$

for which a radially symmetric, Gaussian initial profile remains Gaussian thereafter

$$c(x,y,t)=(4t+1)^{-1}\exp\left[-\left(x^2+y^2\right)/(4t+1)\right]\quad(t\geq 0). \tag{15}$$

To place nodes (x_m,y_m) with local areal densities to match the Gaussian initial concentration field $c(x,y,0)=\exp[-(x^2+y^2)]$, we first fill the unit circle $\xi^2+\eta^2<1$ in an auxiliary (ξ,η) coordinate system with a statistically uniform swarm of points (ξ_m,η_m), and then employ the coordinate transformation

$$x_m=\xi_m F(\xi_m,\eta_m),\quad y_m=\eta_m F(\xi_m,\eta_m),\quad F(\xi,\eta)=\left[\frac{-\ln\left(1-\xi^2-\eta^2\right)}{\xi^2+\eta^2}\right]^{1/2}. \tag{16}$$

Periodic vs. random nodal distributions $\{(\xi_m,\eta_m)\}$ and $\{(x_m,y_m)\}$ are shown in Figure 1.

If the only aim is to obtain local concentrations $c(x,y)$ for a graph, then there is great latitude with regard to the weight function used in Eq. 6. We start with a reasonable choice, the continuously differentiable function

$$w_0(x)=\begin{cases}1-3x^2+2|x|^3, & |x|\leq 1\\ 0, & \text{otherwise}\end{cases} \tag{17}$$

depicted in Figure 2a, and adapt it to either a circular or square averaging zone

$$\text{Circle:}\quad W(x,y) = w\left(\sqrt{x^2+y^2}\right), \quad x^2+y^2<1; \tag{18}$$

$$\text{Square:}\quad W(x,y) = w(x)w(y), \quad |x|<1, |y|<1. \tag{19}$$

The number N_c^* of nodes contained in the averaging area $\mathfrak{A}(\boldsymbol{r};\epsilon)$ should be large enough to quell discretization error in the numerical quadrature 6, yet small enough to prevent macro-scale variations in nodal density from obscuring the local concentration value. To encapsulate the accuracy of the whole numerical concentration profile at a particular instant t, we shall define a root-mean-square deviation

$$\Delta(t) = \left[K^{-1}\sum_{k=1}^{K}\left(\hat{c}(x_k,y_k,t) - c(x_k,y_k,t)\right)^2\right]^{1/2} \tag{20}$$

taken over a fine square grid of K sampling points (x_k, y_k) within a circle of radius $\sqrt{4t+1}$ centered at the origin. Consider the initial distributions of 1,976 and 2,000 nodes depicted in Figures 1b and 1d, respectively. For a circular averaging zone, Figure 3 indicates the variation of $\Delta(0)$ with N_c^* (see Gingold and Monaghan (1982, Figure 2). Once the discretization error in the summation Eq. 6 has died down, the discrepancy scales roughly linearly with N_c^*, which means the second power of ϵ, as should be expected from the integral

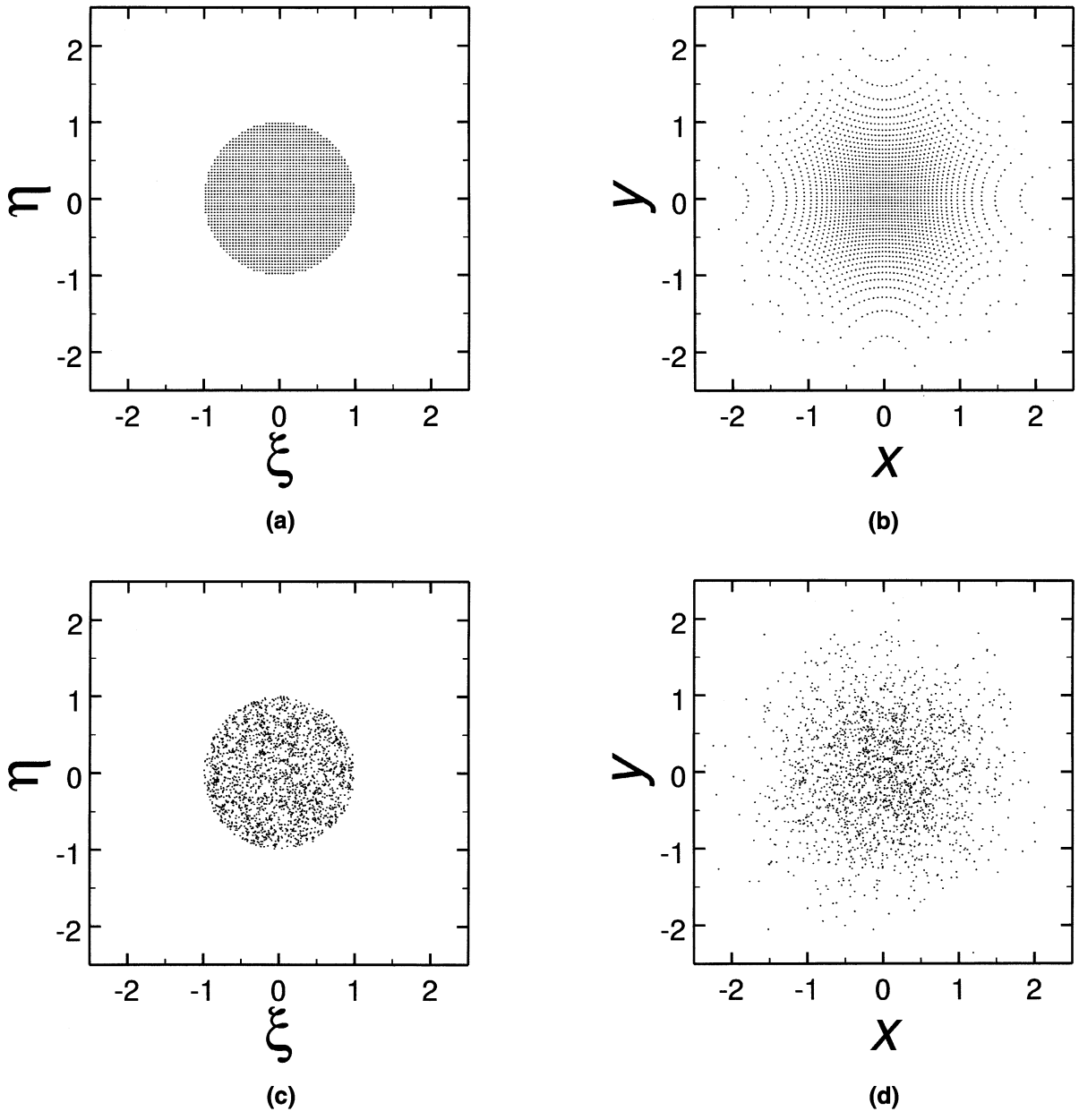

Figure 1. Initial distributions of nodes.

(a) and (c) Regular array of 1,976 nodes vs. random array of 2,000 nodes, both distributed uniformly within the unit circle; (b) and (d) arrays (a) and (c) mapped by Eq. 16 onto the Gaussian distribution of local concentrations $c(x, y, 0)$ from Eq. 15.

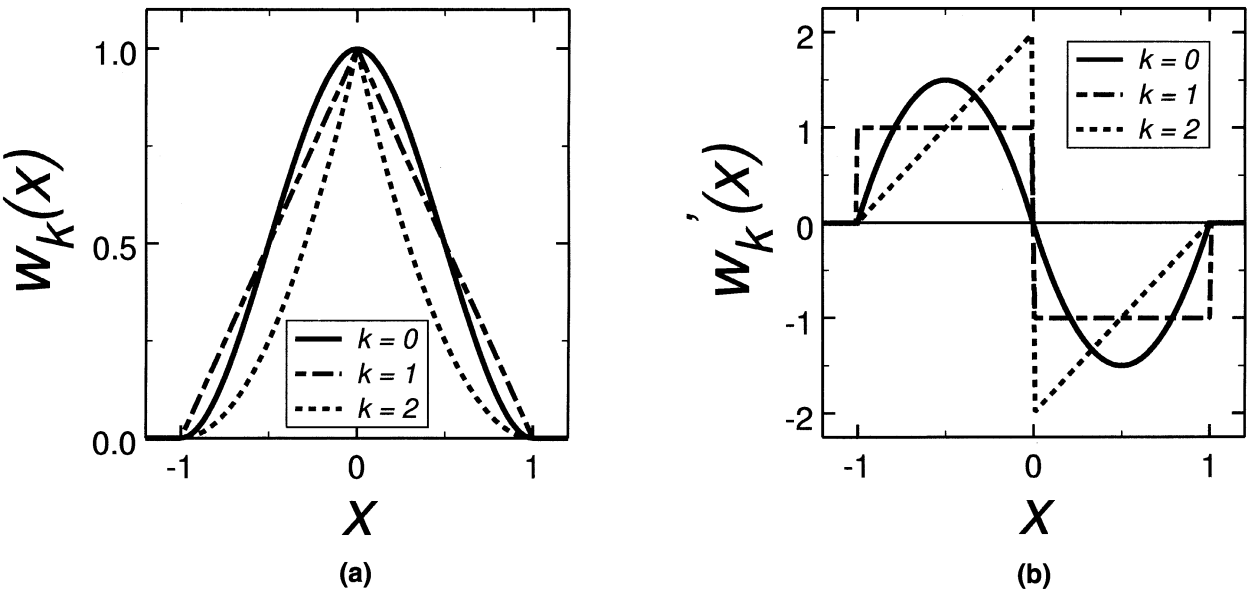

Figure 2. 1-D weight functions from Eqs. 17 and 21 and their slopes.

(a) $w_k(x)$. (b) $w_k'(x)$.

average, 1. Compared with the regular array, the optimal value of N_c^* is larger for the randomly distributed nodes, and the average is less accurate. Thus, we shall confine our attention to regular nodal arrays from here on, and use $N_c^* = 25$ with a circular averaging zone (Eq. 18).

The weight function used to extract the diffusion velocities in the simulations need not coincide with that used to plot concentrations. In fact, when we compare results obtained with different weight functions in Eq. 12, we should make sure to use the same sampling "window" to avoid muddling the effects of varying the former. In addition to the smooth weight function $w_0(x)$, we shall consider the following functions with corners

$$w_k(x) = \begin{cases} (1-|x|)^k, & |x| \le 1 \\ 0, & \text{otherwise} \end{cases} \qquad (k = 1,2). \quad (21)$$

For a circular averaging zone, Figures 4a, 4b, and 4c show how the form of the function $w_k(x)$ affects the nodal trajectories at time $t = 3/8$, starting from the initial nodal positions in Figure 1b. The time step is $\delta t = 1.0 \times 10^{-2}$ in the second-order Runge-Kutta routine. The slope $w_k'(x)$ generates the diffusive flux in response to imbalances in nodal density about the center. In the case of a smooth weight function, such as $w_0(x)$ in Figure 2a, the slope passes through zero at $x = 0$, and thereby gives negligible weight to the nearest nodes (Figure 2b). Instead of causing all nodes to spread apart from one another (the essence of diffusion), it may allow nodes to clump together. For a small sample size ($N_d^* = 50$), this effect is clearly visible in Figure 4a; increasing the sample size ($N_d^* = 100$) helps to alleviate the problem. In general, then, the weight function should have a corner at $x = 0$ so that the slope suffers a discontinuous change in sign. A jump anywhere else in the slope is undesirable, however, because this may again cause nodes to agglomerate into anisotropic patterns (see Figure 4b which shows a simulation based upon the weight function $w_1(x)$ and $N_d^* = 100$). The weight function $w_2(x)$ has the desirable corner at $x = 0$ and is smooth elsewhere: Figure 4c shows that the nodes spread apart evenly from one another, even with the smaller sample size $N_d^* = 50$ for which $w_0(x)$ caused clumping in Figure 4a. Finally, Figure 4d shows a simulation based upon the same weight function $w_2(x)$ fitted to the square averaging area according to Eq. 19. Compared with the radially symmetric weight function 18, some restructuring of the nodal pattern is evident, but this

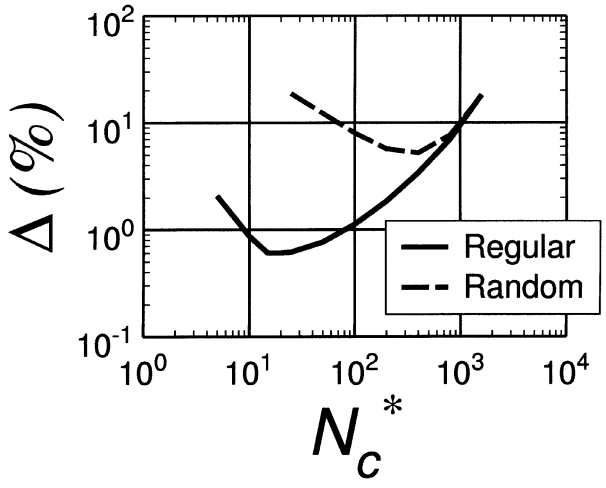

Figure 3. Accuracy Δ of concentrations as a function of sample size N_c^* in the radially-symmetric weight-function average, Eqs. 6, 17, 18, based upon the nodal distributions from Figures 1b and 1d.

Percentages values are scaled to the peak height.

does not have a major effect upon the calculated concentrations: corresponding to Figures 4c and 4d, the values of the deviations $\Delta(3/8)$ are 0.30% and 0.74%, respectively.

Having determined the desirable characteristics of the weight function in Eq. 12—as typefied by $w_2(x)$ and a circular averaging zone—we now turn to the optimal number N_d^* of nodes for this average. Figure 5 shows the effect of N_d^* upon the rms deviation $\Delta(t)$ at three different times as the Gaussian peak spreads. Again, the deviation scales roughly linearly with N_d^* once the discretization error dies down. A reasonable optimum value is $N_d^* = 100$.

With all parameters now roughly optimized for the regular initial array of 1,976 nodes depicted in Figure 1b, Figure 6 shows the concentration profile along the x axis at various times. The numerical concentrations are seen to agree very closely with the analytical solution 15.

Diffusion backward in time is an ill-posed problem, which can lead to violent instabilities in numerics. Thus, one cannot expect the numerical trajectories to be reversible over long times. However, for the progression $[t = 1/10 \rightarrow 1/5 \rightarrow 1/10]$, all particles exhibited essentially reversible trajectories. For the more stringent test $[t = 0 \rightarrow 1/5 \rightarrow 0]$ the particles closest to the center returned to their original vicinity, but deviated noticeably from their starting points. The outer trajectories were, however, essentially reversible. The crucial point is that *ASPH is able (in some cases) to represent the irreversible process of diffusion with reversible trajectories over macroscopic timescales.*

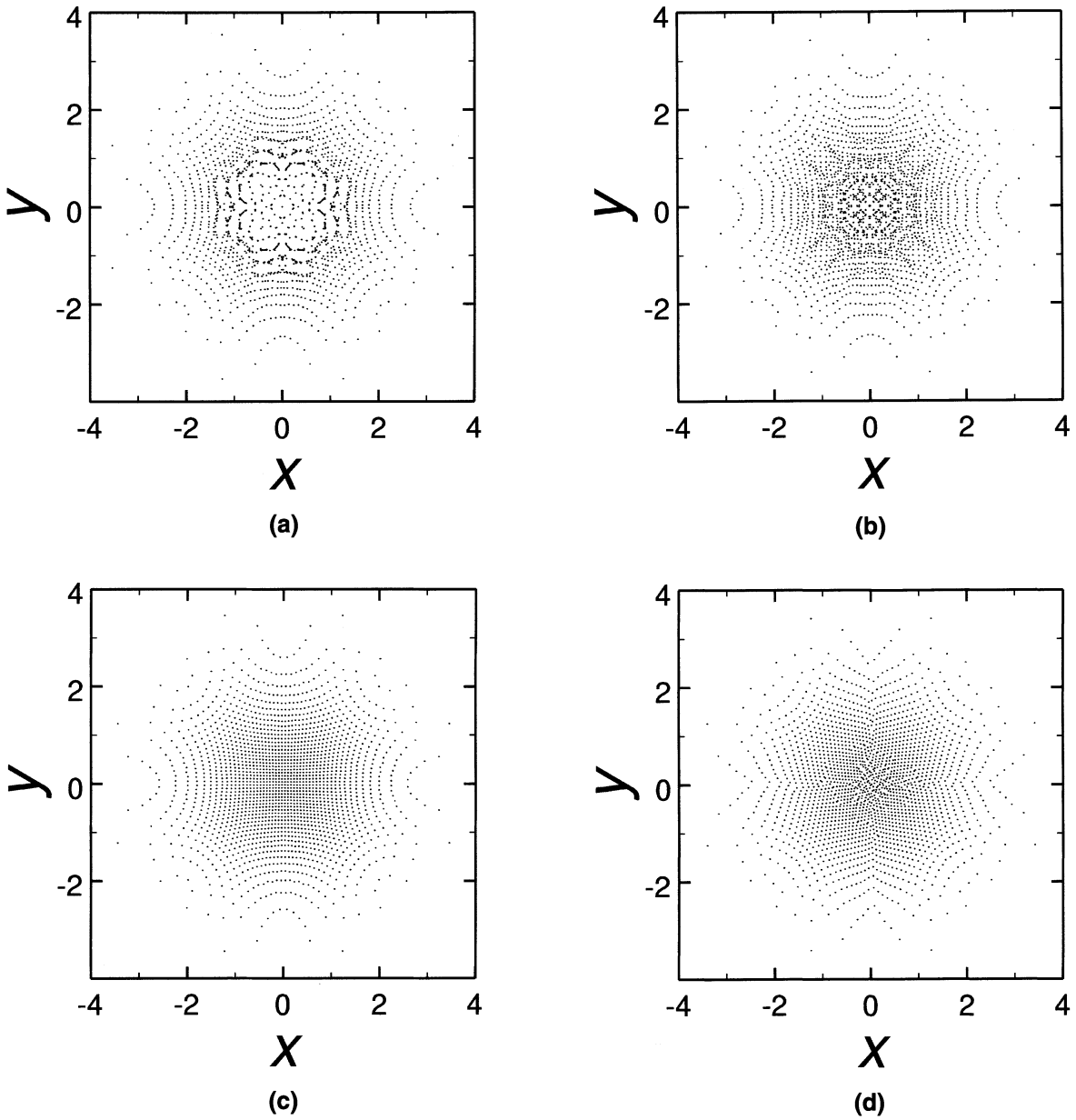

Figure 4. Nodal distributions at $t = 3/8$ starting from the initial condition in Figure 1b.

The time step is $\delta t = 1.0 \times 10^{-2}$. (a) Circle, $w_0(x)$, $N_d^* = 50$. (b) Circle, $w_1(x)$, $N_d^* = 100$. (c) Circle, $w_2(x)$, $N_d^* = 50$. (d) Square, $w_2(x)$, $N_d^* = 100$.

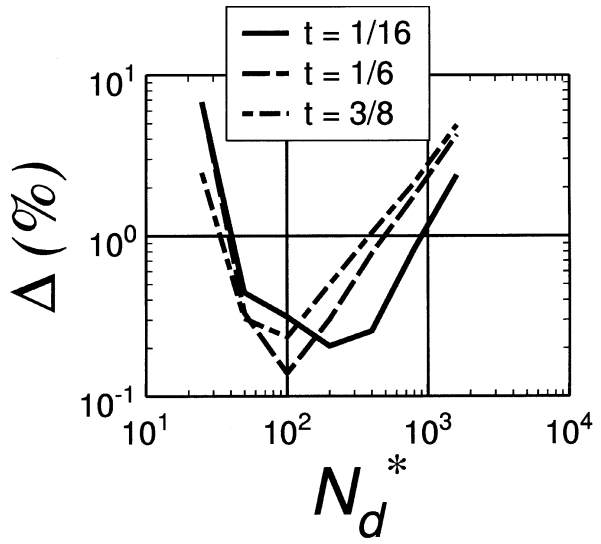

Figure 5. Accuracy $\Delta(t)$ of concentrations plotted as a function of sample size N_d^* in the radially-symmetric weight-function average, Eqs. 12, 18, 21 used to calculate diffusion velocities in the simulations.

Results are plotted for three different times, starting from the initial condition in Figure 1b. Percentages values are scaled to the initial peak height.

Advection-Diffusion in a Rectangular Cavity

Only no-flux boundary conditions will be addressed in this article,

$$\boldsymbol{n}\cdot\boldsymbol{J}=0 \quad \text{on } \partial\mathfrak{D}. \tag{22}$$

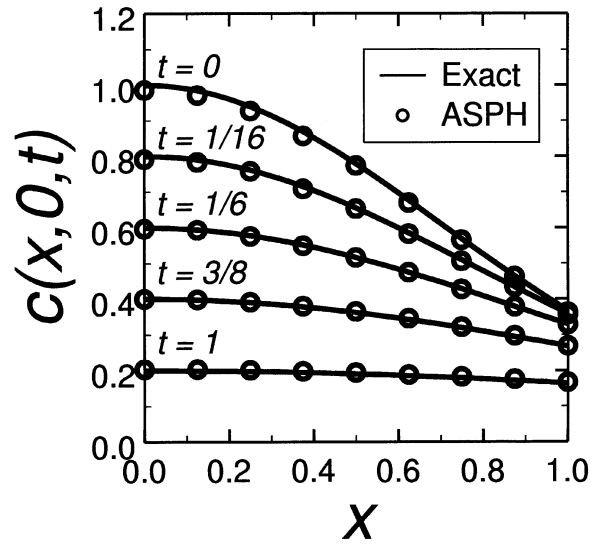

Figure 6. Concentration profiles $c(x,0,t)$ at several times for a simulation starting from the initial condition in Figure 1b.

Circular averaging zone based upon $w_2(x)$; $N_c^*=25$; $N_d^*=100$. The time step is $\delta t=1.0\times10^{-2}$.

These can enforced in a simple, approximate manner by discarding those time steps of individual nodes that would cause them to land outside the domain of solution—whether in the preliminary half-step (predictor), or in the final whole-step (corrector) of the Runge-Kutta scheme. (We defer consideration of more accurate schemes to a subsequent article. Our main aim here is to demonstrate that impermeable boundaries pose no essential problems for ASPH.)

Equation 22 applies at solid walls, and also at the surface of a semipermeable membrane that allows solvent to flow through while rejecting the solute. In other SPH treatments of scalar transport (Cleary and Monaghan, 1999; Chen et al., 1999), the boundaries had to be represented with a less convenient, artificial construction: ghost particles. For a rectangular domain $\mathfrak{D}$, a square averaging area $\mathfrak{A}$, and a multiplicative weight function (Eq. 19) based upon $w_2(x)$, the integrals 2 and 4 for the boundary correction in Eq. 12 can be done analytically.

Both particle swarms and concentration profiles will be shown for ASPH, applied to three incarnations of the generic, dimensionless, 2-D advection-diffusion problem of Eqs. 7 and 8 with no-flux boundary conditions 22 on a rectangular domain $(0<x<1,\ -1/5<y<1/5)$. In each case there were $M=2{,}000$ particles in the simulation, and the target number of particles in the weight-function average 12 was $N_d^*=200$. (For simplicity, the same weight function and the same value for N_c^* were used to compute concentrations in the graphs.) The time step was $\delta t=1.0\times10^{-4}$ in the Runge-Kutta routine; a reasonable level of convergence of the concentrations was spot-verified by doubling δt.

Test problem No. 1

Consider a 1-D ultrafiltration flow with constant diffusivity,

$$u_x(x,y)\equiv 5, \quad u_y(x,y)\equiv 0, \quad D(x,y)\equiv 1. \tag{23}$$

In the context of gravitational sedimentation, the initial condition of a delta-function spike was treated with a routine method by Chandrasekhar (1943). Figure 7 shows how the nodal distribution evolves in time, starting from a central slug composed of a regular array. Solute piles up toward the membrane boundary on the right, until the diffusive back-flux balances advection—the simplest illustration of *concentration polarization.* The numerical concentration profile $\hat{c}(x,0,0.02)$ agrees well with a series solution adapted from Nitsche et al. (1988) (see Figure 8). The numerical error is reasonable but discernibly larger near the ends, where accuracy of the weight-function average degrades from second-order to first-order in ϵ as the averaging zone extends partly outside the domain. Note that the simulations are 2-D, and do not take advantage of the 1-D nature of the problem.

Test problem No. 2

Figure 9 shows the final, steady-state concentration profile when the diffusivity is discontinuous, as would happen, for example, at the junction between two different porous media

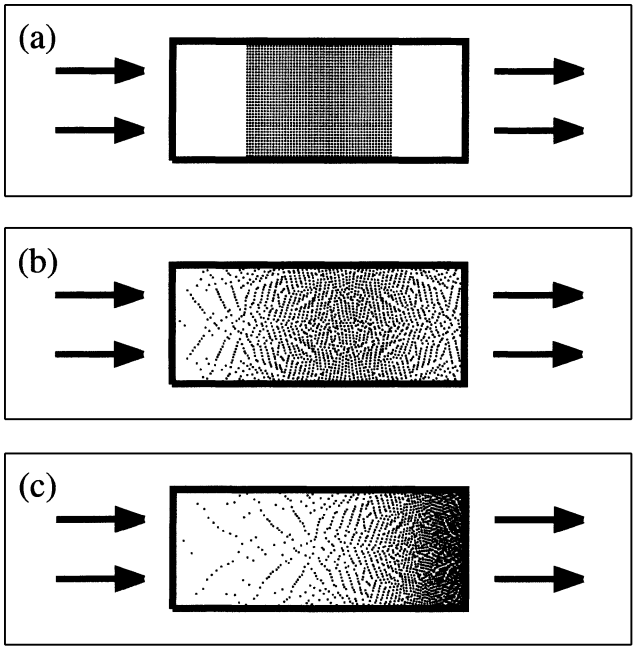

Figure 7. Nodal ultradistributions for ultrafiltration flow in a rectangular domain, Eq. 23.

(a) $t = 0$ (initial). (b) $t = 0.02$. (c) $t = 0.5$ (final).

$$u_x(x,y) \equiv 5, \quad u_y(x,y) \equiv 0,$$
$$D(x,y) = \begin{cases} 1, & x \le 1/2 \\ 10, & x > 1/2. \end{cases} \tag{24}$$

In contrast with the special treatment necessary with conventional SPH (Cleary and Monaghan, 1999), ASPH deals with the discontinuous coefficient automatically.

Test problem No. 3

Finally, Figure 10 shows the final, steady-state distribution of solute for countercurrent flow, in what is now a fully 2-D problem

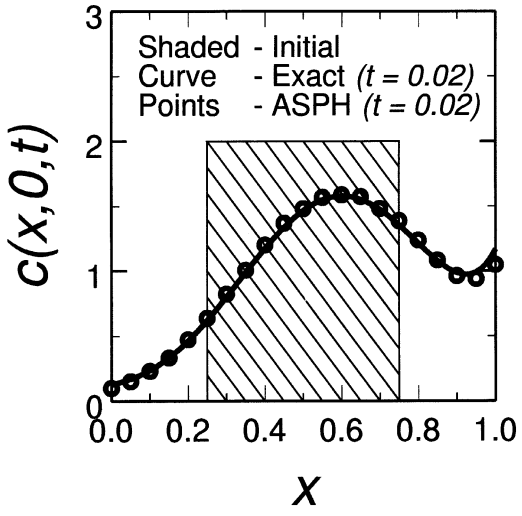

Figure 8. Concentration profile c(x, 0, 0.02) corresponding to Figure 7b.

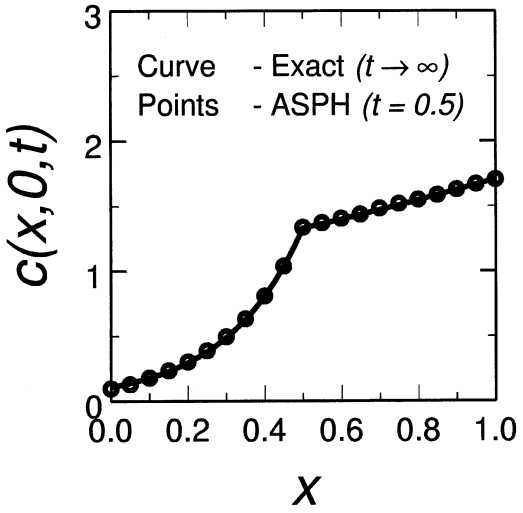

Figure 9. Final, steady-state concentration profile in the case of a discontinuous diffusivity, Eq. 24.

$$u_x(x,y) = \begin{cases} -5, & x < 0 \\ 0, & x = 0, \\ 5, & x > 0 \end{cases} \quad u_y(x,y) \equiv 0, \quad D(x,y) \equiv 1. \tag{25}$$

Here, the advective coefficient is discontinuous. Transverse diffusion (which is assumed here to be unhindered by the longitudinal dialysis membrane that separates the opposing flow streams) is seen to inhibit the advective piling up on the ultrafiltration membranes at the right and left ends. ASPH seems to be ideal for visualizing this phenomenon of *antipolarization dialysis* (Nitsche, 1994, 1995; Nitsche and Zhuge, 1995).

Unified Framework for Diffusion and Interfacial Tension

Expressed in streamlined notation, ASPH allows us to model diffusion of a dilute solute with a swarm of particles whose trajectories are governed by the ODE system

$$\frac{d\boldsymbol{r}_m}{dt} = -D\,\nabla\{\ln[\Phi(\boldsymbol{r}_m)]\}, \quad \Phi(\boldsymbol{r}) = \sum_n W(\boldsymbol{r}_n - \boldsymbol{r}). \tag{26}$$

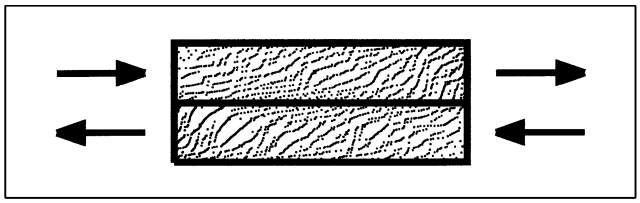

Figure 10. Countercurrent flow, Eq. 25, and the phenomenon of antipolarization dialysis.

Lateral diffusion counteracts longitudinal, advective piling up on the membranes at the left and right. Contrast with the accumulation of solute on the right in Figure 7c.

We now draw a connection with the theory of Nitsche and Schaflinger (2001), whereby inertialess, interfacial-tension-driven flows of drops can also be modeled with a swarm of particles. In a suitable approximation, their corresponding ODE appears in the form

$$\frac{d\boldsymbol{r}_m}{dt} = \alpha\overline{\nabla\{\ln[\Phi(\boldsymbol{r}_m)]\}} + \beta\sum_{n\neq m}\boldsymbol{G}(\boldsymbol{r}_n-\boldsymbol{r}_m)\cdot\overline{\nabla\{\ln[\Phi(\boldsymbol{r}_n)]\}}, \quad (27)$$

with $\boldsymbol{G}$ the Green's function for Stokes flow (point force, fundamental solution, Stokeslet, Oseen-Burgers tensor)

$$\boldsymbol{G}(\boldsymbol{r}) = \frac{1}{8\pi r}(\boldsymbol{I}+\hat{\boldsymbol{r}}\hat{\boldsymbol{r}}), \quad \hat{\boldsymbol{r}} = r^{-1}\boldsymbol{r}, \quad r = \|\boldsymbol{r}\|. \quad (28)$$

By comparing Eqs. 26 and 27, we see that diffusivity and interfacial tension are actually two manifestations of the same thermodynamic driving force $\nabla(\ln\Phi)$. When the forces act directly, we get diffusion, but when the forces act indirectly through the Stokeslet, we get flow driven by interfacial tension. The first term on the righthand side of Eq. 27 originally emerged as a correction for fluid-particle slip, which had the effect of offsetting unphysical expansion of the simulated swarm of particles making up a drop. We can now recognize this contribution as representing a kind of *negative diffusivity* that holds the particles together rather than dispersing them. One caveat mars an otherwise clean analogy: in the case of Stokes flow the forces must be smoothed before using them in the ODE's in order to get good numerical results. The intervening smoothing step is indicated by the overlines in Eq. 27.

The unification of diffusion and Stokes flow opens up the possibility of using Stokeslet-swarm simulations to model transient interfacial tension at the interface between two miscible, interdiffusing liquids (Smith et al., 1981).

Conclusion

This article develops an atomistic version of smoothed particle hydrodynamics that greatly simplifies the implementation for scalar transport problems, and deals automatically with discontinuous coefficients. Four test problems have demonstrated both the accuracy and the versatility of the new method. Finally, diffusion and interfacial tension have been unified under a common conceptual framework.

Point-based methods take numerical analysis one step closer to the underlying subcontinuum physics of the boundary-value problems to which they are applied. The lesson from ASPH, as well as from Stokeslet-based simulations of drops (Machu, 2001; Machu et al., 2001; Nitsche and Schaflinger, 2001), is that even a crude, coarse, highly-stylized representation of nature on the microscopic scale gives good macroscopic results.

Acknowledgments

This article is offered in respectful, affectionate memory of O. Univ.-Prof. Dipl.-Ing. Dr. techn. Uwe Schaflinger, Technical University Graz. Also for Gunther, Walter, Renate, Gerhard, Johnny, Oliver, Thomas, Helfried, Sabine, Karen, Hannah, Janina and Milena, who must carry on without him.

LCN would like to thank Professor Roger Tanner and Professor Nhan Phan-Thien for their kind hospitality at the Dept. of Mechanical and Mechatronic Engineering, University of Sydney, from April to August 2000 (during which time early portions of this work were carried out). Sabbatical support from the University of Illinois at Chicago is gratefully acknowledged. This work was inspired by a wonderful collaboration of LCN with O. Univ.-Prof. Uwe Schaflinger, Dr. Gunther Machu and Professor Walter Meile at the Institute of Fluid Dynamics and Heat Transfer, Technical University Graz.

Literature Cited

Avalos, J. B., and A. D. Mackie, "Dissipative Particle Dynamics with Energy Conservation," *Europhys. Lett.*, **40**, 141 (1997).

Belytschko, T., Y. Krongauz, J. Dolbow, and C. Gerlach, "On the Completeness of Meshfree Particle Methods," *Int. J. Numer. Methods Eng.*, **43**, 785 (1998).

Bird, R. B., W. E. Stewart, and E. N. Lightfoot, *Transport Phenomena*, 2nd ed., Wiley, New York (2002).

Bonet, J., and S. Kulasegaram, "Correction and Stabilization of Smooth Particle Hydrodynamics Methods with Applications in Metal Forming Simulations," *Int. J. Numer. Methods Eng.*, **47**, 1189 (2000).

Campbell, P. M., "Some New Algorithms for Boundary Value Problems in Smoothed Particle Hydrodynamics," *DNA Report DNA-88-286* (1989).

Chandrasekhar, S., "Stochastic Problems in Physics and Astronomy," *Rev. Modern Phys.*, **15**, 1 (1943). [Reprinted in *Selected Papers on Noise and Stochastic Processes*, N. Wax, Ed., Dover, NY (1954).]

Chen, J. K., J. E. Beraun, and T. C. Carney, "A Corrective Smoothed Particle Method for Boundary Value Problems in Heat Conduction," *Int. J. Numer. Methods Eng.*, **46**, 231 (1999).

Clark, A. T., M. Lal, J. N. Ruddock, and P. B. Warren, "Mesoscopic Simulation of Drops in Gravitational and Shear Fields," *Langmuir*, **16**, 6342 (2000).

Cleary, P. W., and J. J. Monaghan, "Conduction Modelling Using Smoothed Particle Hydrodynamics," *J. Comput. Phys.*, **148**, 227 (1999).

Coveney, P. V., and K. E. Novik, "Computer Simulations of Domain Growth and Phase Separation in Two-Dimensional Binary Immiscible Fluids Using Dissipative Particle Dynamics," *Phys. Rev. E*, **54**, 5134 (1996).

Dilts, G. A., "Moving-Least-Squares-Particle Hydrodynamics—I. Consistency and Stability," *Int. J. Numer. Methods Eng.*, **44**, 1115 (1999).

Duarte, C. A., "A Review of Some Meshless Methods to Solve Partial Differential Equations," Technical Report 95-06, TICAM, The University of Texas at Austin (1995).

Español, P., "Hydrodynamics from Dissipative Particle Dynamics," *Phys. Rev. E*, **52**, 1734 (1995).

Español, P., "Fluid Particle Dynamics: A Synthesis of Dissipative Particle Dynamics and Smoothed Particle Dynamics," *Europhys. Lett.*, **39**, 605 (1997a).

Español, P., "Dissipative Particle Dynamics with Energy Conservation," *Europhys. Lett.*, **40**, 631 (1997b).

Español, P., "Fluid Particle Model," *Phys. Rev. E*, **57**, 2930 (1998).

Flekkøy, E. G., and P. V. Coveney, "From Molecular Dynamics to Dissipative Particle Dynamics," *Phys. Rev. Lett.*, **83**, 1775 (1999).

Gingold, R. A., and J. J. Monaghan, "Smoothed Particle Hydrodynamics, Theory and Applications to Non-Spherical Stars," *Mon. Not. Roy. Astr. Soc.*, **181**, 375 (1977).

Gingold, R. A., and J. J. Monaghan, "Kernel Estimates as a Basis for General Particle Methods in Hydrodynamics," *J. Comput. Phys.*, **46**, 429 (1982).

Grassia, P. S., E. J. Hinch, and L. C. Nitsche, "Computer Simulations of Brownian Motion of Complex Systems," *J. Fluid Mech.*, **282**, 373 (1995).

Greenspan, D., "Quasimolecular Simulation of Large Liquid Drops," *Int. J. Numer. Methods Fluids*, **10**, 247 (1990).

Hinch, E. J., private communication.

Hoogerbrugge, P. J., and J. M. V. A. Koelman, "Simulating Microscopic Hydrodynamic Phenomena with Dissipative Particle Dynamics," *Europhys. Lett.*, **19**, 155 (1992).
Jones, J. L., M. Lal, J. N. Ruddock, and N. A. Spenley, "Dynamics of a Drop at a Liquid/Solid Interface in Simple Shear Fields: A Mesoscopic Simulation Study," *Faraday Discuss.*, **112**, 129 (1999).
Koelman, J. M. V. A., and P. J. Hoogerbrugge, "Dynamic Simulations of Hard-Sphere Suspensions Under Steady Shear," *Europhys. Lett.*, **21**, 363 (1993).
Machu, G., "Interfacial Phenomena in Suspensions," Dr. techn. dissertation (U. Schaflinger, advisor), Inst. of Fluid Dynamics and Heat Transfer, Technical University Graz, Graz, Austria (May 2001).
Machu, G., W. Meile, L. C. Nitsche, and U. Schaflinger, "Coalescence, Torus Formation and Breakup of Sedimenting Drops: Experiments and Computer Simulations," *J. Fluid Mech.*, **447**, 299 (2001).
Mackie, A. D., J. B. Avalos, and V. Navas, "Dissipative Particle Dynamics with Energy Conservation: Modelling of Heat Flow," *Phys. Chem. Chem. Phys.*, **1**, 2039 (1999).
Monaghan, J. J., "Smoothed Particle Hydrodynamics," *Ann. Rev. Astron. Astrophys.*, **30**, 543 (1992).
Nitsche, L. C., J. M. Nitsche, and H. Brenner, "Existence, Uniqueness and Regularity of a Time-Periodic Probability Density Distribution Arising in a Sedimentation-Diffusion Problem," *SIAM J. Math. Anal.*, **19**, 153 (1988).
Nitsche, L. C., "Pseudo-Sedimentation Dialysis: An Elliptic Transmission Problem," *Quart. Appl. Math.*, **LII**, 83 (1994).
Nitsche, L. C., "A Singular Perturbation Analysis of Antipolarization Dialysis at High Aspect Ratio," *Indust. Eng. Chem. Res.*, **34**, 3590 (1995).
Nitsche, L. C., and S. Zhuge, "Hydrodynamics and Selectivity of Antipolarization Dialysis," *Chem. Eng. Sci.*, **50**, 2731 (1995).
Nitsche, L. C., and U. Schaflinger, "A Swarm of Stokeslets with Interfacial Tension," *Phys. Fluids*, **13**, 1549 (2001).
Oñate, E., S. Idelsohn, O. C. Zienkiewicz, and R. L. Taylor, "A Finite Point Method in Computational Mechanics. Applications to Convective Transport and Fluid Flow," *Int. J. Numer. Methods Eng.*, **39**, 3839 (1996a).
Oñate, E., S. Idelsohn, O. C. Zienkiewicz, R. L. Taylor, and C. Sacco, "A Stabilized Finite Point Method for Analysis of Fluid Mechanics Problems," *Comput. Methods Appl. Mech. Eng.*, **139**, 315 (1996b).
Öttinger, H. C., *Stochastic Processes in Polymeric Fluids. Tools and Examples for Developing Simulation Algorithms*, Springer, New York (1996).
Pozrikidis, C., *Boundary Integral and Singularity Methods for Linearized Viscous Flow*, Cambridge University Press, New York (1992).
Rallison, J. M., and A. Acrivos, "A Numerical Study of the Deformation and Burst of a Viscous Drop in an Extensional Flow," *J. Fluid Mech.*, **89**, 191 (1978).
Serna, A., J.-M. Alimi, and J.-P. Chieze, "Adaptive Smooth Particle Hydrodynamics and Particle-Particle Coupled Codes: Energy and Entropy Conservation," *Astrophys. J.*, **461**, 884 (1996).
Smith, P. G., T. G. M. van de Ven, and S. G. Mason, "The Transient Interfacial Tension Between Two Miscible Fluids," *J. Colloid Interface Sci.*, **80**, 302 (1981).
Wedgewood, L. E., and K. R. Geurts, "Stochastic Simulation of Transport Phenomena," *Ind. Eng. Chem. Res.*, **34**, 3437 (1995).

Manuscript received July 24, 2000, and revision received Aug. 3, 2001.